RSC Advances

This is an *Accepted Manuscript*, which has been through the Royal Society of Chemistry peer review process and has been accepted for publication.

Accepted Manuscripts are published online shortly after acceptance, before technical editing, formatting and proof reading. Using this free service, authors can make their results available to the community, in citable form, before we publish the edited article. This *Accepted Manuscript* will be replaced by the edited, formatted and paginated article as soon as this is available.

You can find more information about *Accepted Manuscripts* in the Information for Authors.

Please note that technical editing may introduce minor changes to the text and/or graphics, which may alter content. The journal's standard Terms & Conditions and the Ethical guidelines still apply. In no event shall the Royal Society of Chemistry be held responsible for any errors or omissions in this *Accepted Manuscript* or any consequences arising from the use of any information it contains.

ROYAL SOCIETY OF CHEMISTRY

www.rsc.org/advances

Effects of Annealing Ambient on Oxygen Vacancies and Phase Transition Temperature of VO_2 Thin Films

H. Y. Xu[1,2], Y. H. Huang[3], S. Liu[1], K. W. Xu[1,4], F. Ma[1,2,a)], Paul K. Chu[2,a)]

[1] *State Key Laboratory for Mechanical Behavior of Materials, Xi'an Jiaotong University, Xi'an 710049, Shaanxi, China*

[2] *Department of Physics and Materials Science, City University of Hong Kong, Tat Chee Avenue, Kowloon, Hong Kong, China*

[3] *College of Physics and Information Technology, Shaanxi Normal University, Xi'an 710062, Shaanxi, China*

[4] *Department of Physics and Opt-electronic Engineering, Xi'an University of Arts and Science, Xi'an 710065, Shaanxi, China*

RSC Advances Accepted Manuscript

Abstract

VO_2 thin films are prepared on Si substrates by direct-current (DC) magnetron sputtering at room temperature and annealed in vacuum at different argon pressure. The VO_2 thin films annealed in vacuum and Ar are all polycrystalline with a monoclinic structure and after annealing in Ar, the particle size is reduced compared to the films annealed in vacuum. There are more boundaries for smaller particles and so oxygen can more easily diffuse through boundaries resulting in more oxygen vacancies. Annealing under Ar further prevents the samples from

oxidation. As the Ar pressure goes up, the $V2p_{3/2}$ peak broadens and shifts to lower binding energy, implying that there are more oxygen vacancies after annealing. The Raman spectra acquired at room temperature shift to lower frequencies after annealing in Ar further corroborating the existence of oxygen vacancies in the thin films. Raman scattering and resistance measurements show that the critical temperature of the phase transition from monoclinic to tetragonal is reduced from 341 K to 319 K. This can be ascribed to the weaker hybridization between V 3d and O 2p orbitals as a result of oxygen vacancies. Oxygen vacancies affect the phase transition in VO_2 thin films and optical and electrical properties as well.

Keywords: *VO_2; Phase transformation; Oxygen vacancies*

[a] Authors to whom correspondence should be addressed

Electronic mail: mafei@mail.xjtu.edu.cn (F. Ma); paul.chu@cityu.edu.hk (P. K. Chu)

RSC Advances Accepted Manuscript

1. Introduction

Vanadium oxide has various structures due to the multivalent characteristics of vanadium such as V^{2+}, V^{3+}, V^{4+}, and V^{5+} and the metal-insulator transition (MIT) can take place at different temperature depending on the structure. In particular, VO_2 has attracted much interest because of the low MIT transition temperature (T_{MIT}) of 68 °C.[1] Below the critical temperature, VO_2 has a monoclinic phase (M_1, $P2_1/c$) behaving as an insulator, but it transforms to the metallic phase with a tetragonal rutile lattice (r, $P4_2/mnm$) at a temperature higher than the critical value. Since the structural transition is commonly accompanied by abrupt changes in the resistivity, magnetic susceptibility, and optical transmittance,[2-5] VO_2 has potential applications in sensors,[6,7] optical switches,[8,9] and smart windows.[10-12] The phase transition can also be induced by light, electric field, magnetic field, temperature, and stress. Many methods such as atomic layer deposition (ALD),[13] pulsed laser deposition (PLD),[14] chemical vapor deposition (CVD),[15] and sol-gel[16] have been employed to prepare VO_2 thin films and magnetron sputtering is especially attractive because of the low deposition temperature, high film adhesion, and smoothness.

In spite of these attractive properties, use of VO_2 thin films in smart windows is still limited since T_{MIT} is much higher than room temperature. Much research has been conducted to reduce the phase transition temperature by introducing stress/strain,[17,18] changing the chemical stoichiometry,[19,20] and conducitng metal doping.[21] Doping is generally considered to be the most effective method, but it tends to make the process complex and may also introduce stress. Recently, it has been reported that the oxygen content can affect the physical properties of VO_2 thin films.[22,23] Fan *et al*[22] have tried to tune the oxygen vacancy density by changing the

RSC Advances Accepted Manuscript

oxygen flux rate in the molecular beam epitaxy (MBE) process and Jeong *et al*[23] have produced oxygen vacancies in VO_2 thin films by applying an electric field. The transition temperature drops with increasing oxygen vacancies. In previous reports, annealing in a protected atmosphere was shown to produce a less crystallized structure than that annealed in vacuum.[24] In this work, vanadium oxide thin films are prepared by direct current (DC) magnetron sputtering at room temperature and then annealed in Ar. Compared to the films annealed in vacuum, the films annealed in Ar have smaller grain size and more grain boundaries and Ar plays a key role in the formation of oxygen vacancies. The vacancy density increases with Ar pressure and as a result, the transition temperature is lowered substantially. The mechanism is discussed.

2. Experimental details

The vanadium oxide thin films were deposited on Si (100) substrates using direct-current (DC) reactive magnetron sputtering of a V target (99.9% in purity) in a mixed ambient consisting of high-purity oxygen and argon (Ar). Prior to deposition, the substrates were ultrasonically rinsed in acetone and alcohol for 15 min and dried with nitrogen. After the vacuum chamber was evacuated to 1.2×10^{-4} Pa, the substrates were cleaned by Ar sputtering at 0.5 Pa for 5 min with a power of 300 W. Film deposition was then conducted at room temperature for 20 min using a DC power of 220 W at 0.63 Pa. The partial pressure of O_2 and Ar was controlled by mass flow controllers. After deposition, the films were annealed at 450 °C for 2 hours in vacuum as well as in Ar atmosphere with a pressure of 44, 72, and 100 Pa through changing the gas flow from 90 to 190 sccm. The base pressure before thermal annealing is 5 Pa. The important experimental parameters are listed in Table 1.

RSC Advances Accepted Manuscript

The phases of the thin films were determined by grazing-incidence X-ray diffraction (GIXRD, Shimadzu XRD-7000) with Cu K_α radiation (λ = 0.154 nm) at a fixed incident angle of 0.5° and 2θ scanning rate of 8°/min. X-ray photoelectron spectroscopy (XPS, Physical Electronics PHI 5802) with Al K_α irradiation was performed to determine the chemical states and composition. The surface morphology was examined by field-emission scanning electron microscopy (FESEM, JSM-7000F) and atomic force microscopy (AFM, Bruker dimension Icon) employing the tapping mode. Raman scattering was performed on a micro-Raman system (LabRAM HR Evolution, France). A 50X objective lens was used to focus the HeNe laser beam with a wavelength of 514.5 nm onto the VO_2 films and the scattered light was monitored using 1800 g/mm gratings. To avoid unintentional heating during Raman analysis, the incident laser power was small but sufficient to produce an optimal signal-to-noise ratio. The samples were heated from 303 to 343 K at a temperature step of 5 K and the Physical Property Measurement system (PPMS, Quantum Design PPMS-9) was used to determine the electrical resistivity of the films when the temperature was elevated from 293 to 363 K and subsequently reduced back to 293 K with 2 K steps. The sample was fixed and connected to the electrode separately by double-side tape and conductive silver adhesive. The film thickness was measured by SEM and used to calculate the resistivity of the thin films.

3. Result and discussion

The vanadium oxide thin films prepared by DC-reactive magnetron sputtering are homogeneous with a relatively smooth surface. Fig. 1 shows the SEM images revealing the

RSC Advances Accepted Manuscript

morphological difference between as-deposited (Fig. 1(a)) and annealed thin films (Fig. 1(b) and (c)). It is obvious that annealing leads to appreciable change in the surface morphology. Fig. 1(a) reveals that the as-deposited thin films are continuous and smooth whereas Fig. 1(b) shows that the films annealed in vacuum have a porous and fuzzy morphology. As shown in the cross-sectional image in the inset in Fig. 1(b), the films annealed in vacuum consists of columnar particles with an average width of about 25 nm and length of 80 nm. The films annealed in Ar are composed of relatively homogenous and continuous spheroidal nanoparticles with an average diameter of ~14 nm as shown in Fig. 1(c). This is consistent with previously reported results.[24,25] In fact, thermal annealing is accompanied by the reaction of $V_2O_5 \rightarrow 2VO_2 + \frac{1}{2} O_2$. So the nucleation of crystalline VO_2 is more difficult in the oxygen-rich atmosphere. As compared to thermal annealing in vacuum, the oxygen content in the Ar atmosphere is reduced, and consequently the nucleation of VO_2 is promoted. It becomes more significant under higher Ar pressure and leads to smaller grain size. No noticeable difference in the surface roughness is observed from the thin films annealed in different Ar pressure. There are more boundaries when the particles are smaller and hence, it is easier for oxygen to diffuse through the boundaries to increase the oxygen vacancies. Moroever, annealing in Ar prevents the films from oxidation.

The as-deposited thin films are amorphous, and no XRD peak of vanadium oxide could be identified. Furthermore, only a peak at 517.2 eV of V^{5+} is observed from the XPS spectra. So the as-deposited thin films are indeed amorphous V_2O_5. After thermal annealing, some oxygen atoms escape from the thin films with only one peak at 515.8 eV of V^{4+} observed in the XPS spectra, and the thin films become crystallized into VO_2 in M1 phase, as illustrated in the XRD patterns in Fig. 2. Samples 1-4 were prepared at room temperature for 20 min using a DC

RSC Advances Accepted Manuscript

power of 220 W and annealed at different Ar pressure. The O_2/Ar ratio for the fabrication of samples 1-4 is 32.5% as shown in Table 1. Sample 1 annealed in vacuum is designated as 1-V and samples 2-4 annealed at Ar pressure of 44, 72, and 100 Pa are labeled 2-44, 3-72 and 4-100, respectively. Fig. 2(a) shows that the diffraction peaks at 27.86º, 37º, and 55.54º corresponding to the (011), (21-1) and (220) planes of annealed VO_2, respectively. The four samples are all polycrystalline having a monoclinic structure and (011) preferential orientation. The full-width at half-maximum (FWHM) of the (011) peaks in samples 1-V and 2-44 are 0.574^o and 0.732^o respectively. According to Scherrer's formula, the grain size of the VO_2 thin films annealed in Ar is smaller than that annealed in vacuum and it is consistent with the SEM images. However, the grain size changes little after annealing at different Ar pressure. Fig. 2(b) shows the patterns of the VO_2 (011) peaks of samples 1-V and 2-44 marked by light blue square in Fig. 2(a). The red lines are the fitted curves of the experimental data. Compared to sample 1-V, the peak position of sample 2-44 annealed in Ar shifts towards the small-angle direction. The smaller intensity and larger FWHM of the VO_2 (011) peak suggest less crystallization in sample 2-44. Stress in thin films can be categorized into two types: extrinsic stress and intrinsic stress. Thermal stress is an extrinsic one. Because the coefficient of thermal expansion of VO_2 [4.9×10^{-6} ($a_{//}$) or 2.6×10^{-5} K^{-1} ($a_{\perp}$)] is larger than that of Si (3.1×10^{-6} K^{-1}),[26] tensile thermal stress will be induced when the annealing temperature is lowered down to room temperature. However, compressive stress is closely related to the smaller grain size as well as the densification of thin films.[27] Since the particle size in the thin films annealed in Ar is considerably smaller than that annealed in vacuum, compressive stress is produced in the in-plane direction, resulting in decreased in-plane lattice constant and increased out-of-plane lattice constant.[28] Therefore, the

RSC Advances Accepted Manuscript

a-axis on the preferred (011) plane is compressed. The a-axis of monoclinic structure (a_M) corresponds to the c-axis of the rutile structure (c_R). In such a case, the phase transition temperature should be lowered to some degree[29].

The concentration of residual O_2 in the annealing atmosphere decreases with increasing Ar pressure, and the formation of vanadium oxide in higher valence states will be suppressed. This promotes the transformation from V_2O_5 into VO_2 during thermal annealing. In another word, oxygen vacancies are produced in the thin films in order to satisfy the condition of electrical neutrality.[30] Actually, oxygen vacancies are produced through overflowing of oxygen atoms from the thin films to the environment, as $O_O^x \rightarrow v_{\ddot{O}} + 2e^- + \frac{1}{2}O_2(g)$. According to Le Chatelier's principle, the reaction becomes favorable resulting in the formation of oxygen vacancies, if the thermal annealing is carried out in Ar atmosphere. Thus, as the Ar pressure is increased in the thermal annealing process, the oxygen vacancies increase.[31-32] The oxygen vacancies[23] in the VO_2 thin films annealed in Ar are confirmed by XPS. Fig. 3 shows the XPS spectra of samples 1-V, 2-44 and 4-100. The core level binding energy of $V2p_{3/2}$ is usually used to characterize the oxidation state of vanadium and the peak position is fitted by a Gaussian function with the provided XPS software.[33] Compared to the VO_2 thin film annealed in vacuum, the V^{4+} peak shifts to lower energy. When the Ar pressure in the annealing process is further increased, a weak peak at 513.1 eV due to V^{3+} is observed in addition to the strong peak at 515.8 eV of V^{4+}.[34, 35-37] Both the slight shift of V^{4+} peak and appearance of V^{3+} confirm the existence of oxygen vacancy in the thin films annealed in Ar.[38,39] The O:V ratio of the VO_2 thin films annealed in Ar at a pressure of 72 Pa is calculated to be 1.92 and it is 2 for the VO_2 thin films annealed in vacuum. Accordingly, oxygen vacancies exist in the thin films annealed in Ar.

RSC Advances Accepted Manuscript

However, no V_2O_3 phase is observed from the XRD pattern. When the oxygen partial pressure in the sputtering process is further increased (not show here) and annealed in Ar, the XPS spectrum is nearly the same as that of sample 1-V confirming the existence of oxygen vacancies in samples 2-44 to 4-100.

The oxygen vacancies in the VO_2 thin films annealed in Ar are further assessed by Raman scattering. Fig. 4 (a) shows the room-temperature Raman spectra of samples 1-V and 4-100. At 303 K, there are 7 Raman peaks at 195 (A_g), 224 (A_g), 261 (B_g), 310 (A_g), 391 (A_g), 439 (B_g), and 616 cm^{-1} (A_g) characteristic of the M1 phase of VO_2 and the peak at 520 cm^{-1} originates from the Si substrate. The three prominent phonon modes at frequencies of 195, 224, and 616 cm^{-1} are denoted ω_{v1}, $\omega_{v2,}$ and ω_0. ω_{v1} and ω_{v2} are attributed to vibration of V–V and the high-frequency mode, ω_0, is due to vibration of V–O. The peaks of sample 4-100 marked by the black square in Fig. 4(a) shift to lower frequencies compared to sample 1-V as shown in Fig. 4(b). Parker et. al[40] found that the Raman peaks shifted to lower frequencies in V-riched thin films. Fig. 4(c) presents the Raman spectra of sample 4-100 in the temperature range from 303 to 338 K. As the annealing temperature goes up, the intensity of all the Raman peaks decreases gradually. When the temperature is higher than 323 K, the M1 phase is no longer detected and the VO_2 thin films transform into the tetragonal phase with no Raman peak accompanied by the semiconductor-to-metal transition. Fig. 5 shows the electrical resistivity of the samples as a function of temperature and the corresponding derivatives of resistivity with respect to temperature. The black and red curves correspond to the heating and cooling cycles, respectively. The thin films are heated in vacuum from room temperature to 363 K and then cooled to room temperature in steps of 2 K. T_{MIT} is defined as the minimum value of dR/dT

RSC Advances Accepted Manuscript

and the hysteresis width (△H) is defined as the difference in T_{MIT} in the heating and cooling processes. All the samples exhibit phase transition from a high resistance state to a metallic state and thermal hysteresis. Fig. 6 shows the T_{MIT} and hysteresis width obtained from the curve of resistivity as a function of temperature. The resistance of sample 1-V changes by more than three orders of magnitude in the process, and T_{MIT} is 341 K with a smaller hysteresis width of 4 K, which is consistent with previously reported results.[1,41] However, when the thin films are annealed in Ar, both T_{MIT} and the change in resistance decrease. As reported before, the grain size plays a role in broadening the hysteresis width and reducing T_{MIT}.[42] The smaller grain size commonly leads to the larger hysteresis width due to the small density of nucleating defects and the large interfacial energies.[43] However, the samples have similar grain size when they are annealed at different Ar pressure. Hence, the grain size is not the dominant factor in determining T_{MIT}. Goodenough et al[44] have pointed out that oxygen vacancies in non-stoichiometric thin films may reduce the transition temperature due to extra free electrons [45,46]. As shown in Fig. 5, the films annealed in Ar (samples 2-44 to 4-100) are more conductive than those annealed in vacuum at room temperature indicating electron doping. The chemical states and hybridization of V3d and O2p electrons may reveal information about the influence of oxygen vacancies on the phase transition in VO_2. Below the MIT transition temperature, the V and O atoms in the monoclinic phase are strongly bonded with each other *via* hybridization between the V 3d and O 2p orbitals and the films are insulating. After annealing in Ar, oxygen vacancies are generated to weaken hybridization between V 3d and O 2p, and the partial loss of V^{4+}-V^{4+} bonding lowers the temperature for the metal-insulator transition. It was also found that oxygen vacancies could stabilize R phase even at room temperature and thus reduce the activation energy and phase transition temperature. Hence, bond breaking and reforming

RSC Advances Accepted Manuscript

become easier and the phase transition temperature is reduced substantially.

4. Conclusion

In summary, polycrystalline VO_2 thin films with the monoclinic structure are prepared on Si substrates by DC magnetron sputtering. The oxygen content can be reduced by annealing in Ar and so more oxygen vacancies are produced. Raman scattering and electrical resistance measurements in the temperature range between 293 K and 363 K demonstrate that T_{MIT} of the VO_2 thin films decreases from 335 K to 319 K with increasing oxygen vacancies. Our study reveals that annealing in Ar is a simple and effective approach to produce oxygen vacancies in VO_2 thin films and lower the phase transition temperature.

Acknowledgements

This work was jointly supported by National Natural Science Foundation of China (Grant No. 51271139, 51471130, 51302162), Fundamental Research Funds for the Central Universities, and City University of Hong Kong Applied Research Grant (ARG) Nos. 9667104 and 9667122.

References

[1] F. J. Morin, *Phys. Rev. Lett*. 1959, 3, 34.

[2] A. Cavalleri, T. Dekorsy, H. H. W. Chong, J. C. Kieffer, and R. W. Schoenlein, *Phys. Rev. B,* 2004, 70, 161102(R).

[3] W. Li, J. J. Zhu, J. R. Liang, Z. G. Hu, J. Liu, H. D. Chen, and J. H. Chu, *J. Phys. Chem. C*, 2011, 15, 23558-23563.

RSC Advances Accepted Manuscript

[4] W. T. Liu, J. Cao, W. Fan, Z. Hao, M. C. Martin, Y. R. Shen, J. Wu, and F. Wang, *Nano Lett*. 2011, 11, 466-470.

[5] R. Lopez, T. Haynes, L. Boatner, L. Feldman and R. Haglund, *Phys. Rev. B*, 2002, 65, 224113, 1-5.

[6] J. Wu, Q. Gu, B. S. Guiton, N. P. de Leon, L. Ouyang and H. Park, *Nano Lett*. 2006, 6, 2313-2317.

[7] Z. Li, H. Zhang, W. Zheng, W. Wang, H. Huang, C. Wang, A. G. MacDiarmid and Y. Wei, *J. Am. Chem. Soc*. 2008, 130, 5036-5037.

[8] W. X. Huang, X. G. Yin, C. P. Huang, Q. J. Wang, T. F. Miao, and Y. Y. Zhu, *Appl. Phys. Lett*. 2010, 96, 261908.

[9] C. Chen and Z. Zhou, *Appl. Phys. Lett*. 2007, 91, 011107.

[10] C. G. Granqvist, B. Pehlivan, Y. X. Ji, S. Y. Li and G. Niklasson, *Thin Solid Films*, 2014, 559, 2-8.

[11] C. G. Granqvist, *Sol. Energy Mater. Sol. Cells*, 2007, 91, 1529-1598.

[12] S. Y. Li, G. A. Niklasson, and C. G. Granqvist, *Thin Solid Films*, 2012, 520, 3823-3828.

[13] K. Martens, I. P. Radu, S. Mertens, X. Shi, L. Nyns, S. Cosemans, P. Favia, H. Bender, T. Conard, M. Schaekers, S. De Gendt, V. Afanas'ev, J. A. Kittl, M. Heyns and M. Jurczak, *J. Appl. Phys*. 2012, 112, 124501.

[14] J. Sakai, M. Zaghrioui, V.T. Phuoc, S. Roger, C. Autret-Lambert and K. Okimura, *J. Appl. Phys*. 2013, 113, 123503.

[15] D. Vernardou, D. Louloudakis, E. Spanakis, N. Katsarakis and E. Koudoumas, *Sol. Energy Mater. Sol. Cells*, 2014, 128, 36-40.

[16] J. Wu, W. X. Huang, Q. W. Shi, J. H. Cai, D. Zhao, Y. B. Zhang and J. Z. Yan, Appl. *Surf.*

RSC Advances Accepted Manuscript

Sci. 2013, 268, 556-560.

[17] J. H. Park, J. Coy, T. Kasirga, C. Huang, Z. Fei, S. Hunter and D. Cobden, *Nature*, 2013, 500 ,431-434.

[18] J. Cao, E. Ertekin, V. Srinivasan, W. Fan, S. Huang, H. Zheng, J. W. L. Yim, D. R. Khanal, D. F. Ogletree, J. C. Grossman and J. Wu, *Nat. Nanotechnol*. 2009, 4, 732-737.

[19] S. X. Zhang, I. S. Kim and L. J. Lauhon, *Nano Lett*. 2011, 11, 1443-1447.

[20] J. Jeong, N. Aetukuri, T. Graf, T. D. Schladt, M. G. Samant and S. S. P. Parkin, *Science*, 2013, 339, 1402-1405.

[21] N.R. Mlyuka, G.A. Niklasson and C.G. Granqvist, *Appl. Phys. Lett*. 2009, 95, 171909, 1-3.

[22] L. L. Fan, S. Chen, Y. F. Wu, F. H. Chen, W. S. Chu, X. Chen, C. W. Zou and Z. Y. Wu, *Appl. Phys. Lett*. 2013, 103, 131914-131914-5.

[23] J. Jeong, N. Aetukuri, T. Graf, T. D. Schladt, M. G. Samant and S. S. P. Parkin, *Science*, 2013, 339, 1402 -1405.

[24] D.W. Liu, Y. Y. Liu, B. B. Garcia, Q. F. Zhang, A. Pan, Y. Jeong and G. Zh. Cao, J. Mater. Chem., 2009, **19**, 8789-8795.

[25] D. Zhang, L. B. Su, H. J. Li, X. B. Qian and J. Xu, J. Cryst. Growth, 2006, 294, 437.

[26] K. Okimura, T. Watanabe and J. Sakai, *J. Appl. Phys*. 2012, **111**, 073514.

[27] N. H. Azhan, K. Su, K. Okimura and J. Sakai, *J. Appl. Phys*. 2015, **117**, 185307.

[28] D. P. Zhang, M. D. Zhu, Y. Liu, K. Yang, G. X. Liang, ZH. H. Zheng and X. M. Cai, *Journal of Alloys and Compounds*, 2016, 659, 198-202.

[29] L. L. Fan, S. Chen, Z. L. Luo, Q. H. Liu, Y. F. Wu, L. Song, D. X. Ji, P. Wang, W. S. Chu, C. Gao, C. W. Zou and Z. Y. Wu, *Nano Lett*, 2014, 14, 4036-4043.

[30] X. X. Liu, SH. W. Wang, F. L. Chen, L. M. Yu and X. SH. Chen, *J. Phys. D: Appl. Phys*.

RSC Advances Accepted Manuscript

2015, 48, 265104.

[31] B. Lucas-Granados, R. Sanchez-Tovar and R. M. Fernandez-Domene, *J. Garcia-Anton, Solar Energy Materials & Solar Cells*, 2016, 153, 68–77.

[32] B. Sarma, A. L. Jurovitzki, R. S. Ray, Y. R. Smith, S. K. Mohanty and M. Misra, *Nanotechnology*, 2015, 26, 265401.

[33] G. Silversmit, D. Depla, H. Poelman, G.B. Marin, and R.D. Gryse, *J. Electron Spectrosc. Relat. Phenom*. 2004, 135, 167-175.

[34] Y. Q. Lv, M. Hu, M. Wu and ZH. Liu, Surface & Coatings Technology, 2007, 201, 4969-4972.

[35] N. Alov, D. Kutsko, I. Spirovova and Z. Bastl, *Surf. Sci*. 2006, 600, 1628-1631.

[36] D. H. Youn, H. T. Kim, B. G. Chae, Y. J. Hwang, J. W. Lee, S. L. Maeng, and K. Y. Kang, *J. Vac. Sci. Technol. A*, 2004, 22, 719-724.

[37] G. A. Sawatzky and D. Post, *Phys. Rev. B*, 1979, 20, 1546.

[38] Z. T. Zhang, Y. G. Gao, Z, Chen, J. Du, C. Cao, L. Kang and H. J. Luo, *Langmuir*, 2010, 26, 10738-10744.

[39] R. V. Vovk, M. A. Obolenskii, A. A. Zavgorodniy, A. V. Bondarenko, I. L. Goulatis, A.V. Samoilov, A. Chroneos, *J. Alloys Comp*. 2008, 453, 69-74.

[40] J. C. Parker , *Phys. Rev. B*, 1990, 42, 3164.

[41] Z. F. Luo, X. Zhou, D. W. Yan, D. Wang, Z. Y. Li, C. B. Yang, Y. D. Jiang, *Thin Solid Films* 2014, 550, 227-232.

[42] M. J. Miller, J. Wang, *Journal of Applied Physics*, 2015, 117, 034307.

[43] H. F. Zhang, ZH. M. Wu, Q. He and Y. D. Jiang, *Applied Surface Science*, 2013, 277, 218-222.

RSC Advances Accepted Manuscript

[44] J. B. Goodenough, *J. Solid State Chem.* 1971, 3, 490–500.

[45] D. Ruzmetov, S.D. Senanayake, V. Narayanamurti and S. Ramanathan, *Phys. Rev. B* 2008, 77, No. 195442.

[46] C. C. Y. Kwan, Ch. Griffith and H. K. Eastwood, *Appl. Phys. Lett*. 1972, 20, 93–95.

RSC Advances Accepted Manuscript

Table Ⅰ. Samples annealed at different Ar pressure.

Sample	1	2	3	4
O2/Ar Sputtering	32.5%	32.5%	32.5%	32.5%
Ar pressure (Pa) (annealing)	0	44	72	100

RSC Advances Accepted Manuscript

Figure Captions

FIG. 1. SEM images of VO2 thin films: (a) As-deposited and (b)-(c) Annealed in vacuum and Ar, respectively. The inset in (b) is the corresponding cross-sectional image showing columnar particles with an average width of 25 nm and length of 80 nm. (c) The film has relatively homogenous and continuous spheroidal nanoparticles with an average diameter of ~14 nm.

FIG. 2. (a) X-ray diffraction patterns of the vanadium oxide thin films 1 to 4 deposited with the ratio of O_2/Ar of 32.5% followed by annealing at different Ar pressure of 0, 44, 72, and 100 Pa, respectively. Sample 1-4 are designated as 1-V, 2-44, 3-72, 4-100, respectively. (b) Fine pattern of (011) peaks of sample 1-V and 2-44. The red lines are the fitted curves of the experiment data.

FIG. 3. Comparision between the high-resolution V 2P XPS spectra of thin films 1-V, 2-44, and 4-100. The V^{4+} peak shifts to lower energy as the Ar pressure is raised.

FIG. 4. (a) Raman spectra of sample 1-V and 4-100 measured at room temperature. (b) Raman spectra of sample 4-100 as the function of temperature between 303 and 338 K

FIG. 5. (a), (c) Resistivity of the VO_2 thin films as the function of temperature for samples 1-V and 4-100. The differential curves (b) and (d) are used to determine the phase transition characteristics including T_{MIT} and hysteresis width.

FIG. 6. Comparison of the phase transition properties derived from the differential of

RSC Advances Accepted Manuscript

resistivity-temperature curves: (a) T_{MIT} and (b) hysteresis width.

RSC Advances Accepted Manuscript

Fig. 1

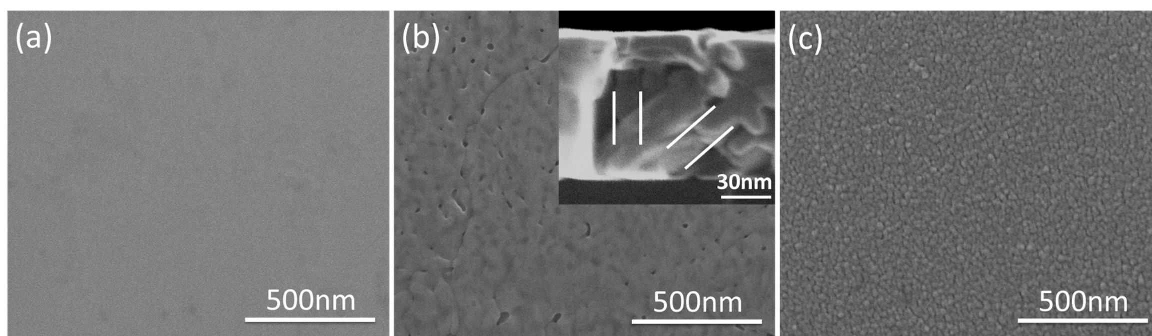

RSC Advances Accepted Manuscript

Fig. 2

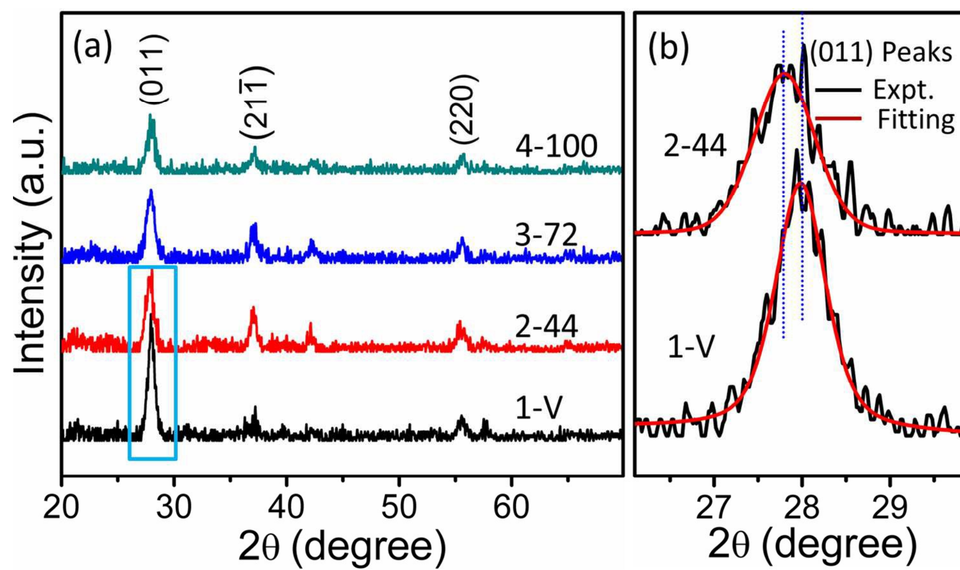

RSC Advances Accepted Manuscript

Fig. 3

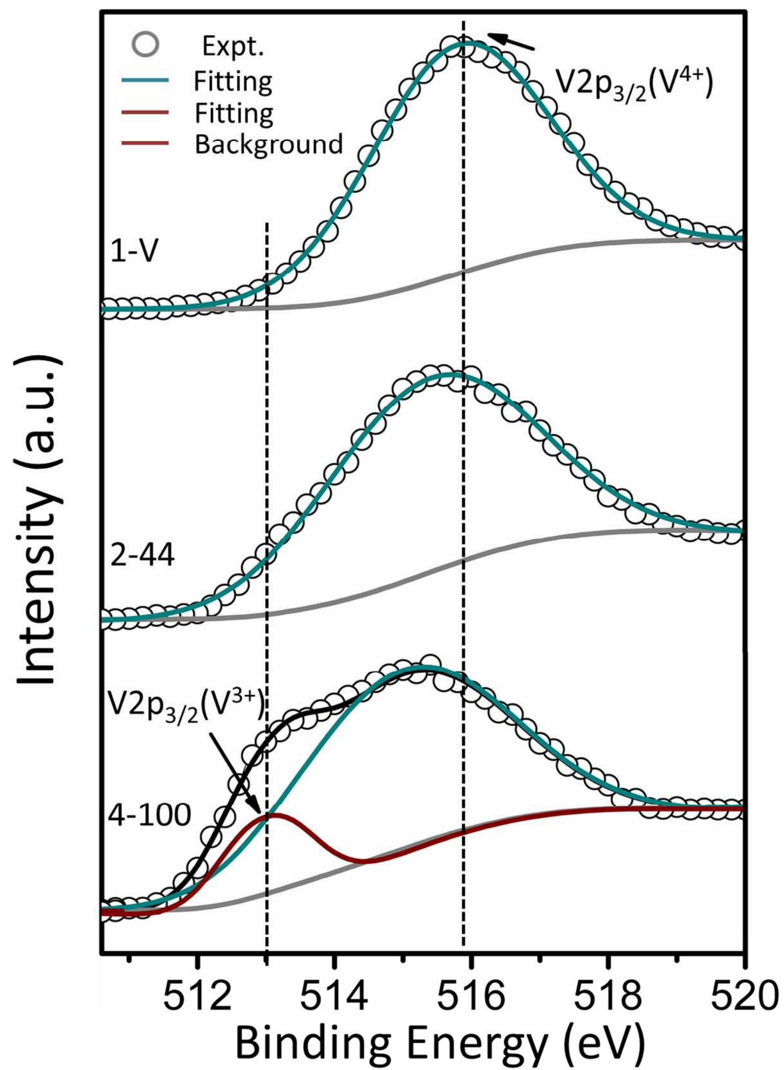

RSC Advances Accepted Manuscript

Fig. 4

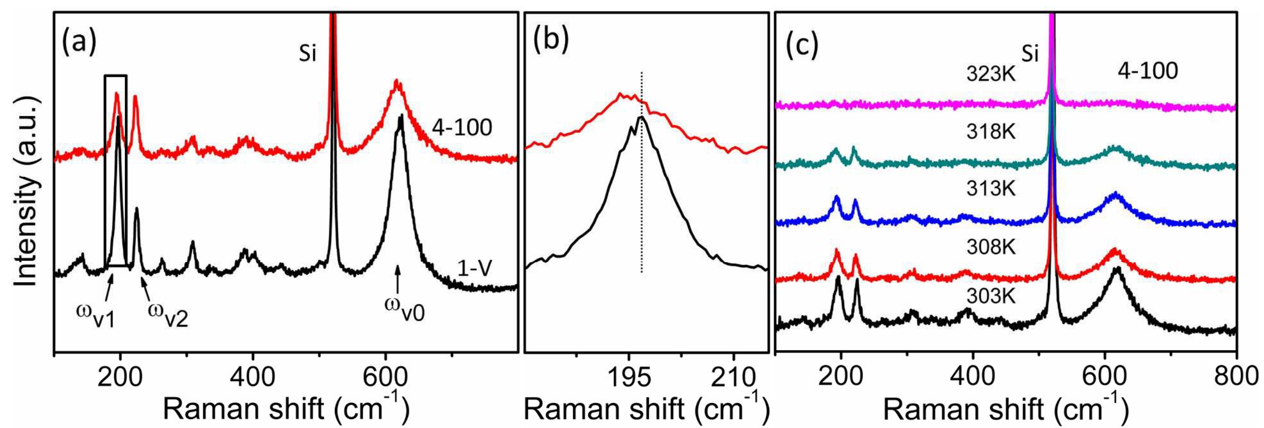

RSC Advances Accepted Manuscript

Fig. 5

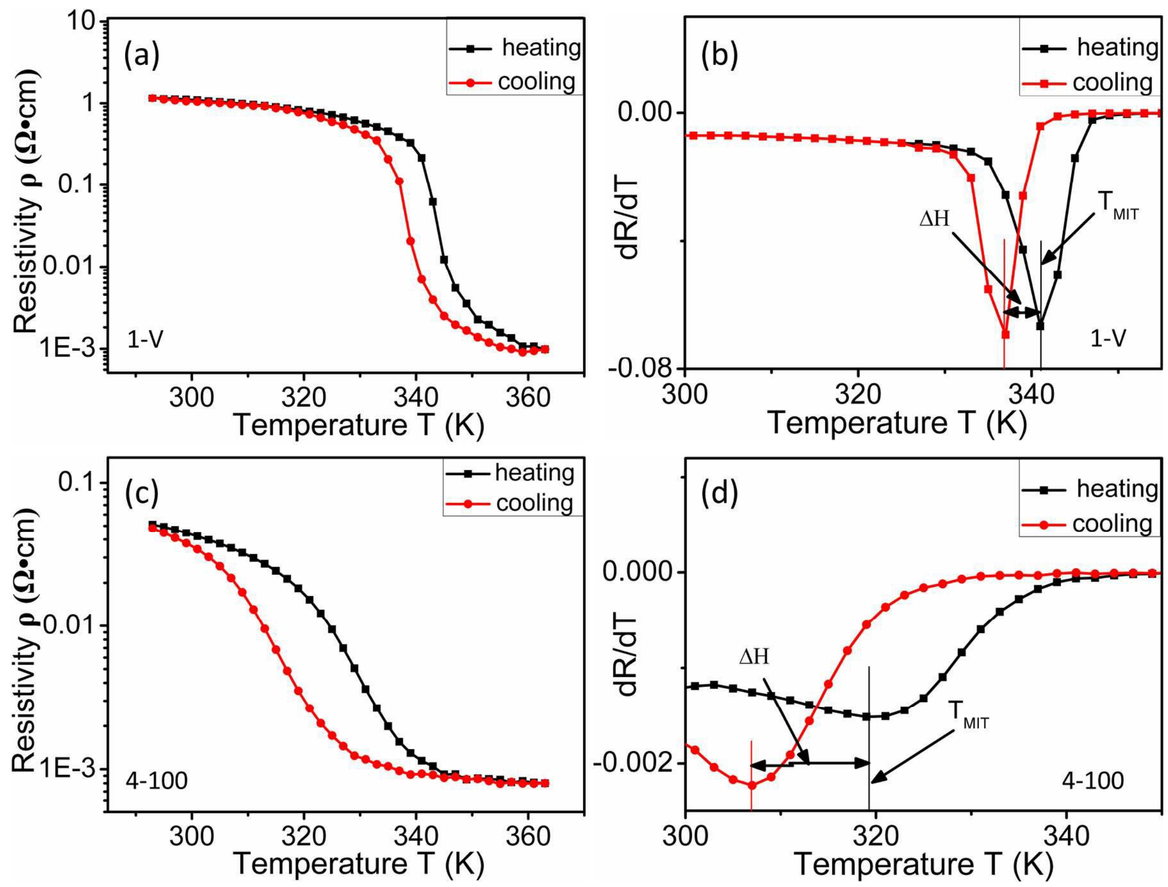

RSC Advances Accepted Manuscript

Fig. 6

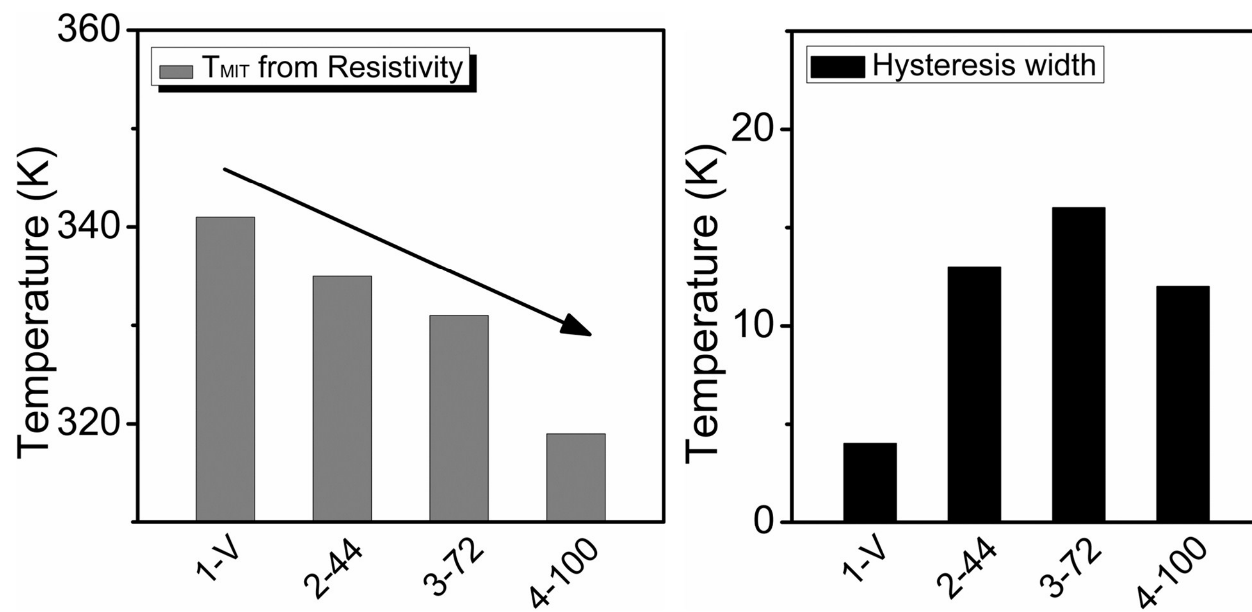

RSC Advances Accepted Manuscript